American Mineralogist, Volume 87, pages 1415–1425, 2002

High-pressure behavior of bikitaite: An integrated theoretical and experimental approach

ORAZIO FERRO,[1] SIMONA QUARTIERI,[2,*] GIOVANNA VEZZALINI,[1] ETTORE FOIS,[3] ALDO GAMBA,[3] AND GLORIA TABACCHI[3]

[1]Dipartimento di Scienze della Terra, Largo S. Eufemia, 19, I-41100 Modena, Italy
[2]Dipartimento di Scienze della Terra, Salita Sperone 31, I-98166 Messina-S.Agata, Italy
[3]Dipartimento di Scienze Chimiche, Fisiche e Matematiche, Università dell'Insubria, via Lucini 3, I-22100, Como, Italy

ABSTRACT

Pressure-induced structural modifications in the zeolite bikitaite are studied by means of in situ synchrotron X-ray powder diffraction and ab initio molecular dynamics. The experimental cell parameters were refined up to 9 GPa, at which pressure we found reductions of 4.5, 4.5, 6.3, and 15% in *a*, *b*, *c*, and *V*, respectively. Minor variations were observed for the cell angles. Complete X-ray amorphization is not achieved in the investigated *P* range, moreover the *P*-induced effects on the bikitaite structure are completely reversible. Because it was possible to extract only the cell parameters from the powder patterns, the atomic coordinates at 5.7 and 9.0 GPa were obtained by means of Car-Parrinello simulations using the unit-cell parameters experimentally determined at these pressures. Analysis of the computational results for increasing pressures showed that the volume contraction is essentially due to rotations of the tetrahedra; the 8-ring channels become more circular; the pyroxene chain becomes more corrugated in the *b*-*c* plane; and the mean Li-O bond distances and coordination polyhedral volumes decrease with increasing pressure without significant distortion of the internal angles. The peculiar aspect of the bikitaite structure, i.e., the presence in the channels of a "floating" one-dimensional water chain, is only partially maintained at high pressure; the compression brings framework O atoms close enough to water hydrogen atoms to allow the formation of host-guest hydrogen bonds, without, however, destroying the one-dimensional chain.

INTRODUCTION

Bikitaite [$Li_2(Al_2Si_4O_{12})\cdot 2H_2O$, s.g. *P*1] is a high-density zeolite with Li as the extra-framework cation. Its topology, also observed in the synthetic aluminosilicate compound $Cs_{0.35}Al_{0.35}Si_{2.65}O_6$ (Annehed and Fälth 1984), is characterized by parallel sheets with hexagonal tiling, connected by pyroxene chains developing along *b*. Also parallel to *b*, the structure is characterized by a system of mono-dimensional non-crossing channels, each delimited by 8-membered rings. This channel system alternates along *a* with high-density *b*-*c* layers. The two Li cations present in the bikitaite unit cell are coordinated to one water molecule and three framework O atoms, although the two water molecules are hydrogen bonded to each other and form a peculiar one-dimensional chain, parallel to the channel direction. No hydrogen bonds have been found between water and the framework (Ståhl et al. 1989). Recent studies (Quartieri et al. 1999; Fois et al. 1999) demonstrated the high rigidity and stability of the water chain and excluded room temperature rotational motion of water molecules, therefore justifying the naming of such a water system as "one-dimensional ice." Moreover, the same authors demonstrated that the water-chain system is stabilized by host-guest interactions based on the antiparallel dipole moments of the framework and the water chain.

Bikitaite represents an example of confinement of a low-dimensionality system in an ordered matrix (Fois et al. 2001a, 2001b), which could be of technological relevance for the tailoring of new kinds of materials with particular chemical and physical properties. In this respect, it is highly desirable to study the stability of this system under different physico-chemical conditions, in order to understand how low-dimensional species can be introduced and stabilized in materials like zeolites. To this aim, we undertook a multi-technique investigation on the structural modifications in bikitaite at high-temperatures (H*T*) (Vezzalini et al. 2001b) and high-pressures (H*P*).

Although the thermal behavior of zeolites has been extensively studied (see for example Bish 1995), the scientific literature on the effects of pressure, using penetrating or non-penetrating pressure-transmitting media, is limited. Little information is available on the structural properties and on the possible pressure-induced polymorphic phases, although more effort has been dedicated to the study of the amorphization processes and of pressure-induced effects on ionic conductivity. Most of the available information is on fibrous zeolites (Belitsky et al. 1992; Gillet et al. 1996; Bazhan et al. 1999; Goryainov and Smirnov 2001; Lee et al. 2002; Moroz et al. 2001; Ballone et al. 2002), analcime and wairakite (Hazen and Finger 1979; Velde and Besson 1981; Goryainov et al. 1996, 1999), heulandite (Comodi et al. 2001; Vezzalini et al. 2001a), and synthetic zeolites A and Y (Hazen 1983; Hazen and Finger 1984; Huang 1998; Secco and Huang 1999).

* E-mail: simonaq@unimo.it

Here we present the results of an experimental (in situ synchrotron X-ray powder diffraction, XRPD) and theoretical (ab initio molecular dynamics, MD) study on the behavior and stability of bikitaite and its one-dimensional water system under pressure. In this type of approach - already used to study scolecite at H*P* (Ballone et al. 2002) and bikitaite at H*T* (Vezzalini et al. 2001b) – the experimental and computational techniques complement each other in the most favorable way, with structural parameters and phase boundaries determined by the experimental measurements, whereas the computational method is used to interpret and model with atomistic resolution the structural changes that occur in the zeolite with increasing pressure.

EXPERIMENTAL METHODS

The bikitaite sample used in this work is from Bikita, Zimbabwe. The cell parameters at room *P* and *T* are a = 8.606(1) Å, b = 4.9573(4) Å, c = 7.5970(7) Å, α = 89.94(6)°, β = 114.407(9)°, and γ = 89.98(5)°. The space group was assumed to be *P*1, on the basis of the structural refinements performed on samples from Bikita and North Carolina by Bissert and Liebau (1986) and by Quartieri et al. (1999), respectively.

The XRPD experiments were performed at beamline ID09 at ESRF (European Synchrotron Radiation Facilities), at a fixed wavelength of 0.43103 Å, using a diamond anvil cell and silicon oil (Gillet et al. 1996; Le Bihan et al. 1996) as the non-penetrating pressure-transmitting medium. A known problem deriving from the use of non-penetrating media is their limited range of hydrostaticity. However, silicon oil, already used in other H*P*-studies of zeolites (Gillet et al. 1996; Gatta et al. 2001; Vezzalini et al. 2001a; Ballone et al. 2002), can be considered satisfactory up to at least 5 GPa, on the basis of results obtained on heulandite using both glycerol (Comodi et al. 2001) and silicon oil (Vezzalini et al. 2001a). Moreover, Le Bihan et al. (1996) studied several intermetallic uranium compounds under high pressure with different pressure-transmitting media (silicon oil, ethanol-methanol-water, and liquid argon). Stress due to the solidification of silicon oil was observed at about 9 GPa, but in the lower pressure range no significant difference was observed with respect to the other pressure-transmitting media.

The pressures were measured by the ruby fluorescence method (Mao et al. 1986) on the non-linear hydrostatic pressure scale. The estimated error in the pressure values is 0.1 GPa. The experiments were performed from P_{amb} up to 9.9 GPa with ΔP increments of ~1 GPa and ~2 GPa in the ranges P_{amb} – 5.7 GPa and 5.7 – 9.9 GPa, respectively. Additional data was collected upon decompression, at 2.7 and 0.1 GPa. A MAR345 detector (pixel dimension 100 μm) was placed 367.97 mm away from sample, and the exposure time was 64.6 s for all pressures. The sample was rocked by ±3° increments in ω in order to reduce texture in the diffraction images. One-dimensional diffraction patterns were obtained in the 2θ range 2–25° by integrating the two dimensional images with the program FIT2D (Hammersley et al. 1996) and are shown in Figure 1.

The peak intensities of the collected patterns are not reliable because they are significantly influenced by a number of uncontrollable effects, such as the poor statistics of the diffraction data (due to the low mosaicity of the crystallites and the small volume hit by the beam) and the development of strong preferred orientations. As a consequence, it was not possible to refine the crystal structures and only the unit-cell parameters were extracted from the powder patterns by means of the Rietveld method. The unit-cell refinements were carried out in the 2θ range 2–18° up to 9 GPa by means of the GSAS program (Larson and Von Dreele 1994). The coordinates of the adopted structural model are those refined by Vezzalini et al. (2001b) from the synchrotron X-ray powder pattern collected on the same bikitaite sample at room conditions at the GILDA beamline (ESRF, Grenoble). The background curves were fitted by a Chebyshev polynomial with a number of coefficients related to the worsening of features with increasing pressures; namely 18 at P_{amb}, 21 from 0.9 to 7.5 GPa, 22 from 7.5 to 9.0 GPa. The pseudo-Voight profile function proposed by Thomson et al. (1987) was used with refined Gaussian (GW) and Lorentzian (LY) terms. The asymmetry correction from Finger et al. (1994) was used up to the 5.7 GPa, above which the broadening of peaks did not allow any correction. The refined cell

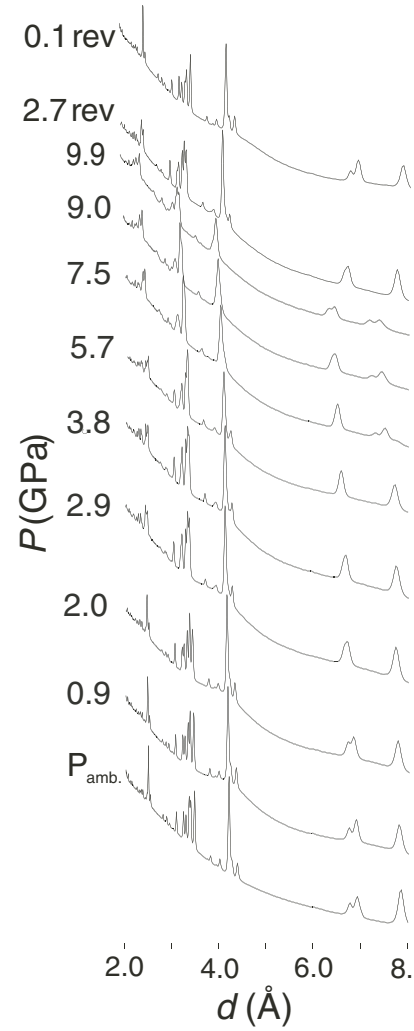

FIGURE 1. Integrated powder patterns of bikitaite as a function of pressure.

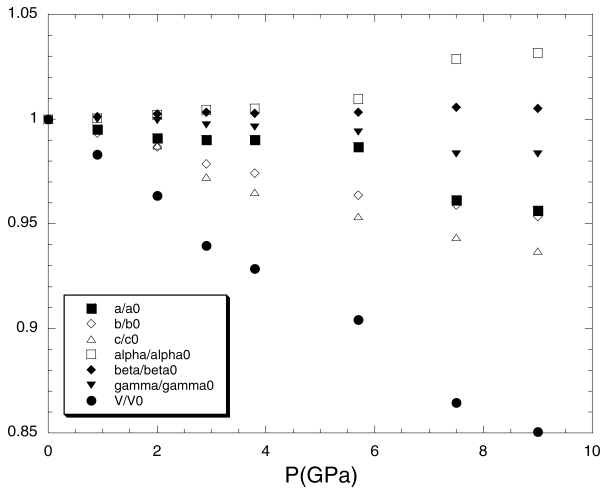

FIGURE 2. Experimental unit-cell parameters normalized to room condition values vs. pressure. The errors on the cell parameters are smaller than the symbols used.

parameters as a function of pressure are reported in Table 1 and Figure 2.

COMPUTATIONAL METHOD

In order to investigate the H*P*-induced deformations in bikitaite structure at a microscopic scale we adopted the ab initio molecular dynamics (MD) approach of Car and Parrinello (1985). This is an advanced Density Functional Theory-based computational technique particularly suited for ab initio simulations of condensed phase systems; in particular, it was previously used to study the stability of bikitaite structure at atmospheric temperature and pressure (Fois et al. 1999; Quartieri et al. 1999) and its thermal behavior (Vezzalini et al. 2001b). Detailed descriptions of the theoretical basis for this approach have been reported in several publications and reviews (see Parrinello 1997).

We present here the results from two simulations obtained by using the cell parameters determined at 5.7 and 9.0 GPa, respectively, and compare them with previous simulations at ambient conditions, from Fois et al. (1999) and Quartieri et al. (1999). The same computational environment was used in order to make comparisons significant. In particular, the simulations were performed in the *NVE* ensemble, with constant volume *V*, number of particles *N*, and total energy *E*.

In our calculations we used an MD supercell consisting of 2 crystallographic unit cells along the *b* direction. Therefore, the chemical formula of our periodically repeated bikitaite MD cell is $2 \times (Li_2Al_2Si_4O_{12} \cdot 2H_2O)$.

The electronic structure is calculated by density functional theory (Kohn 1999; Kohn and Sham 1965), using the gradient corrected functionals proposed by Becke (1988) and Perdew (1986) for the exchange and correlation energies, respectively. Only valence electrons are explicitly described in the computation, and their interaction with the ionic core (nuclei + core electrons) is modeled by norm conserving pseudopotentials (Kleinmann and Bylander 1982; Troullier and Martins 1991). Periodic boundary conditions are used for the simulations. The simulation parameters (e.g., fictitious mass, time step) and the computer code (Hutter et al. 1990, 1996) are the same as those used by Fois et al. (1999) and Quartieri et al. (1999).

The MD simulations were performed using a cut-off of 816 eV, the same as used for simulations at ambient conditions. For both MD runs, the time evolution of the system was followed for 5 ps after equilibration. The average temperature of the simulations was 298 K for both pressures, because the experimental cell parameters were determined at room temperature. In addition, we performed energy optimization for fixed atomic positions using a cut-off of 1224 eV, in order to have an accurate comparison of the total energies among the three average bikitaite structures (i.e., at 5.7 GPa, at 9 GPa, and at ambient conditions), which are characterized by different cell volumes. The structural parameters (distances, angles, and radial distribution functions) obtained from a shorter MD experiment on bikitaite at 5.7 GPa with a cut-off of 1224 eV, were found to be identical to the ones obtained using a value of 816 eV, thus confirming that the use of this cut-off ensures reliable structural data.

In principle, it would also be possible to calculate cell parameters at given *T* and *P* from first principles, and to compare them with the corresponding experimental values. However, such calculations would require carrying out Car-Parrinello simulations in the *NPT* ensemble (i.e., with constant number of particles, temperature, and pressure), in which the cell parameters are dynamical variables and may change during the simulation (Parrinello and Rahman 1981). We did not perform these *NPT* calculations as they would require a much higher plane wave cut-off than the one adopted, with a consistent increase in computational costs; moreover, such a procedure is not essential to obtain reliable coordinates once cell parameters are known.

EXPERIMENTAL RESULTS

Figure 1 shows that the peak intensities decrease and the peak profiles become broader with increasing pressure, suggesting increasing long-range structural disorder. However, complete X-ray amorphization is not achieved in the investigated *P* range. From the decompression powder patterns, reported in the same figure, it can be concluded that the *P*-induced effects on the bikitaite structure are completely reversible. This is confirmed by the excellent agreement between the cell parameters measured during compression and those at the decompression pressures of 2.7 and 0.1 GPa (Table 1).

Even though the powder patterns maintain, as a whole, the same features for all pressures, the low θ diffraction peak (100) shows a progressive split between 7.5 and 9.9 GPa; likewise an additional splitting concerning (001) is also observed at 9.9 GPa. After a careful study of these features, the nucleation of new phases was excluded, because no correspondence was found with diffraction lines of known compounds. Moreover, attempts to attribute these splits to possible superstructures were unsuccessful. Next, three Rietveld refinements of the 9.9 GPa pattern were carried out, using in one both components of the split peaks and in the others the disjointed components of the

(100) and (001) diffractions. The cell parameters refined in the three assumed models were equal within 3σ. It is worth noting that the split observed in the two low θ peaks is not visible at higher θ, however the peak broadening does not allow us to rule out its presence. This evidence suggests the presence in the powder of two very similar lattices, which could be due to the appearance of a metastable phase. Because of the uncertainty of these cell parameters, they are not reported in Table 1. The refined lattice parameters at 7.5 and 9.0 GPa were considered to be more reliable, because of the better pattern quality and minor degree of peak broadening (quantified in terms of smaller GW profile coefficients).

Figure 2 shows the pressure-dependence of the lattice parameters of bikitaite. The largest contractions in the range 0–9 GPa are observed for the cell volume (15%) and *c* parameter (6.3%); *a* and *b* contract by 4.5%, whereas minor variations are observed in the cell angles. In general, the pressure-dependence trends are almost linear up to 5.7 GPa, whereas slight slope variations are observed above this pressure, especially for *a* and α. Linear regressions yielded the following compressibility values: $\beta_a = 2.1(4)\cdot10^{-3}$, $\beta_b = 6.4(3)\cdot10^{-3}$, $\beta_c = 8.7(7)\cdot10^{-3}$, $\beta\alpha = -1.7(1)\cdot10^{-3}$, $\beta_\beta = -0.6(2)\cdot10^{-3}$, and $\beta_\gamma = 1.1(1)\cdot10^{-3}$. The isothermal bulk modulus $K_0 = 45(1)$ was determined up to 5.7 GPa, using a second-order Birch-Murnaghan equation of state (Birch 1952).

COMPUTATIONAL RESULTS

As previously discussed, we did not attempt any structure refinement from the XRPD patterns and, hence, the following discussion will be based on the atomic positions obtained by simulations.

The crystallographic coordinates of bikitaite at 5.7 and 9 GPa were obtained by calculating the time average of the instantaneous atomic positions from the corresponding MD trajectories. The projections of these bikitaite average structures on the *a-c* and *a-b* planes are shown in Figures 3 and 4 respectively, together with those of bikitaite calculated at ambient conditions. The calculated atomic positions of bikitaite are reported in Table 2. From these data it can be seen that at both 5.7 and 9 GPa, the largest variations are shown by the *y* and *z* values.

Framework and lithium polyhedron

All the geometrical data reported in Tables 3–6 were calculated by averaging the instantaneous values calculated at each MD step over the simulation times. For comparison, the corresponding values calculated at room pressure (Quartieri et al. 1999) are also reported in the cited Tables. In particular, Tables 3 and 4 report the mean tetrahedral T-O bond distances, O-T-O and T-O-T angles, respectively; tetrahedral volumes and standard deviations σ are shown in Figure 5. The mean internal O-T-O angles of the tetrahedra are constant up to the highest pressure; the mean T-O distances and tetrahedral volumes show a slight decrease with pressure, although their variations are all within 2σ. In particular, Si23 and Al13 show the largest volume contraction and dispersion of O-T-O angle values.

Because the total volume contraction of the bikitaite unit cell (about 15%) is much higher than the tetrahedral contraction, the main cause of the *P*-induced structural modifications are the rotations of the quasi-rigid tetrahedral units: all the bridging inter-tetrahedra T-O-T angles become smaller as the volume decreases (Table 4), with a mean T-O-T contraction of about 10 degrees from ambient pressure to 9 GPa. This finding is in agreement with what is generally observed for other framework silicates under pressure (Ross 2000) and allows us to define the bikitaite framework as collapsible, on the basis of the rigid unit model (Baur 1995; Dove et al. 1995; Hammond et al. 1997a, 1997b, 1998).

A further issue concerning the bikitaite framework is that at both room pressure (Ståhl et al. 1989; Quartieri et al. 1999) and high pressure the Si-O-Al angles are strongly affected by the coordination to Li cations, with the average Si-O-Al angle for Li-coordinated O atoms lower than that for non-coordinated O atoms.

The pyroxene chain, which runs along *b,* becomes more corrugated in the *b-c* plane: the O14-O24-O14 angle changes from 131.8° at room pressure to 120.3° at 5.7 GPa, and then to 117.5° at 9 GPa, thus affecting both *b* and *c*. With increasing pressure, the 8-membered ring channels in the *a-c* plane become more circular (Fig. 3), with a resulting greater decrease of *c* with respect to *a* (Table 1, Fig. 2). Figure 4, which displays a projection of the bikitaite structure on the *a-b* plane, clearly shows the large deformation of the hexagonal tiling, accomplished by rotation of the Si23 and Al13 tetrahedra. These features are related to the deformation of the hexagonal layer as a whole, which could be described with alternating "regular" and "deformed" tetrahedral strips. These strips are the projections in the *a-b* plane of the high-density and low-density layers alternating along the *a* direction. Remarkably, the O atoms of the deformed strips are largely involved in the lithium coordination and in hydrogen bonds with the water molecules, as discussed below.

TABLE 1. Experimental unit cell parameters from powder patterns at different pressures

P (GPa)	*a* (Å)	*b* (Å)	*c* (Å)	α (°)	β (°)	γ (°)	*V* (Å³)
P_{amb}	8.6061(11)	4.9573(4)	7.5970(7)	89.94(6)	114.407(9)	89.98(5)	295.14(6)
0.9	8.5641(11)	4.9250(4)	7.5619(8)	89.97(8)	114.542(10)	89.98(6)	290.13(6)
2.0	8.5294(15)	4.8920(5)	7.5003(10)	90.13(7)	114.685(13)	89.92(5)	284.36(7)
2.9	8.5228(12)	4.8517(4)	7.3868(11)	90.33(4)	114.795(12)	89.731(18)	277.28(7)
3.8	8.5214(12)	4.8295(5)	7.3320(8)	90.41(4)	114.724(9)	89.650(17)	274.07(6)
5.7	8.4932(16)	4.7773(6)	7.2443(9)	90.804(29)	114.794(13)	89.442(20)	266.81(7)
7.5	8.2725(33)	4.7560(12)	7.1676(19)	92.53(11)	115.066(25)	88.48(5)	255.18(15)
9.0	8.231(5)	4.7320(19)	7.1187(30)	92.80(15)	114.99(4)	88.37(8)	251.02(23)
2.7rev	8.5391(13)	4.8719(5)	7.4215(10)	90.39(4)	114.826(10)	89.718(18)	280.21(7)
0.1rev	8.6080(10)	4.9568(4)	7.5963(7)	89.848(25)	114.426(8)	89.947(23)	295.11(5)

TABLE 2. Crystallographic coordinates

	1 atm			5.7 GPa			9.0 GPa		
	x	y	z	x	y	z	x	y	z
Li1	0.2965	0.3307	0.1531	0.2982	0.3199	0.1751	0.3002	0.2841	0.1852
Li2	0.6648	0.8312	0.8256	0.6555	0.8082	0.8008	0.6485	0.7621	0.7962
Si11	0.0888	0.8186	0.0680	0.0875	0.7992	0.0723	0.0922	0.7631	0.0853
Si12	0.0854	0.8013	0.4793	0.0857	0.8384	0.4885	0.0941	0.8915	0.4982
Si22	0.8563	0.2972	0.4525	0.8606	0.3324	0.4513	0.8544	0.3888	0.4499
Si23	0.6000	0.3492	0.0473	0.5999	0.3498	0.0468	0.5971	0.3143	0.0367
Al13	0.3500	0.8515	0.9033	0.3500	0.8508	0.9069	0.3505	0.8238	0.9189
Al21	0.8730	0.3181	0.8854	0.8677	0.2957	0.8793	0.8657	0.2567	0.8645
O11	0.2427	0.6978	0.0316	0.2411	0.6696	0.0283	0.2467	0.6216	0.0366
O12	0.0577	0.1463	0.0327	0.0674	0.1378	0.0398	0.0772	0.0977	0.0223
O13	0.1365	0.7520	0.3005	0.1467	0.7072	0.3055	0.1479	0.7189	0.3288
O14	0.0231	0.5134	0.5318	0.0085	0.5745	0.5688	-0.0124	0.6605	0.5707
O15	0.2414	0.9245	0.6560	0.2398	0.9920	0.6632	0.2489	0.0130	0.6971
O16	0.4411	0.1616	0.0355	0.4527	0.1430	0.0773	0.4782	0.0977	0.1010
O21	0.7020	0.2022	0.9372	0.6992	0.1697	0.9384	0.6994	0.1341	0.9276
O22	0.9016	0.6699	0.9377	0.8984	0.6534	0.9328	0.8981	0.6234	0.9468
O23	0.8065	0.2515	0.6370	0.8008	0.2102	0.6157	0.7991	0.2295	0.6001
O24	0.9173	0.0122	0.4016	0.9351	0.0710	0.3586	0.9605	0.1499	0.3580
O25	0.7047	0.4224	0.2675	0.7098	0.4896	0.2576	0.7013	0.5081	0.2480
O26	0.5217	0.6345	0.9289	0.5004	0.6064	0.8938	0.4819	0.5529	0.8559
O17	0.3951	0.2779	0.4472	0.4031	0.2613	0.4661	0.4054	0.2867	0.4742
O27	0.5634	0.7773	0.5357	0.5533	0.7582	0.5047	0.5563	0.7820	0.4981
H11	0.3186	0.2389	0.5052	0.3385	0.2245	0.5456	0.3607	0.3042	0.5785
H12	0.4695	0.1230	0.4807	0.4725	0.0907	0.4828	0.4742	0.1096	0.5030
H21	0.6439	0.7638	0.4792	0.6213	0.7397	0.4272	0.6182	0.8049	0.4166
H22	0.4995	0.6111	0.5012	0.4943	0.5769	0.4872	0.4951	0.6033	0.4604

Note: Nomenclature of the atoms as in Ståhl et al. (1989).

TABLE 3. T-O distances

	1 atm	5.7 GPa	9.0GPa		1 atm	5.7 GPa	9.0 GPa
Si11-O (Å)				**Si12-O (Å)**			
Si11-O11	1.638	1.627	1.623	Si12-O13	1.640	1.633	1.629
Si11-O12	1.638	1.628	1.626	Si12-O14	1.647	1.640	1.646
Si11-O13	1.647	1.648	1.639	Si12-O15	1.619	1.617	1.605
Si11-O22	1.641	1.637	1.618	Si12-O24	1.647	1.638	1.634
average	1.641	1.635	1.626	average	1.638	1.632	1.629
Si22-O (Å)				**Si23-O (Å)**			
Si22-O14	1.651	1.625	1.622	Si23-O16	1.637	1.630	1.631
Si22-O23	1.614	1.623	1.621	Si23-O21	1.637	1.631	1.621
Si22-O24	1.646	1.646	1.639	Si23-O25	1.662	1.661	1.656
Si22-O25	1.649	1.631	1.639	Si23-O26	1.637	1.618	1.635
average	1.640	1.631	1.630	average	1.643	1.635	1.636
Al13-O (Å)				**Al21-O (Å)**			
Al13-O11	1.787	1.757	1.764	Al21-O12	1.796	1.776	1.768
Al13-O15	1.780	1.776	1.765	Al21-O21	1.798	1.781	1.773
Al13-O16	1.746	1.799	1.790	Al21-O22	1.792	1.779	1.772
Al13-O26	1.784	1.771	1.779	Al21-O23	1.769	1.761	1.753
average	1.775	1.776	1.787	average	1.789	1.774	1.767

The geometrical features of the lithium coordination polyhedra are reported in Table 5, whereas the trend of the Li tetrahedra volume is shown in Figure 5. Both mean Li1-O and Li2-O bond distances and the polyhedral volumes decrease with increasing pressure, without significant distortion of the internal tetrahedral angles. The Li-O_{frame} distances decrease less than the Li-O_{water} distances. It is worth noting that the Li2 tetrahedron, which is smaller than the Li1 tetrahedra at room pressure, becomes the largest at high pressure. This seems to be due to the fact that the bond distance Li2-O26 is not particularly affected by increasing pressure, with O26 being the only O atom of the lithium tetrahedra also involved in an H-bond with a water molecule.

Water system

Bond distances and angles of the water system in bikitaite as a function of pressure are reported in Table 6. The water molecule's geometry is almost unaffected by pressure: the O-H bonds do not vary appreciably, and the H-O-H bond angles increase slightly during compression. Interestingly, the one-dimensional water chain structure, typical of bikitaite, is still present under high pressure. However, significant variations are computed for the water-water (O17-O27) and O_{water}···· H intermolecular distances as a function of pressure, reflecting modifications in the H-bonding system along the water chain. All these findings can be rationalized by observing that, because the one-dimensional water chain develops along the *b* axis, contraction along this axis brings about a shortening of both the O_{water}····O_{water} and hydrogen bond distances and a change in the O_{water}····O_{water} ····O_{water} angle. Moreover, the O_{water}····H - O_{water} angles are significantly affected by pressure: the average angle changes from 170.3° (ambient pressure) to 161.7° at 5.7 GPa, and a further decrease to 157.9° is observed at 9 GPa. As a consequence the chain becomes more corrugated in the *bc*

TABLE 4. O-T-O and T-O-T angles

	1 atm	5.7 GPa	9.0 GPa		1 atm	5.7 GPa	9.0 GPa
O-Si11-O (°)				O-Si12-O (°)			
O11-Si11-O12	109.97	108.40	105.49	O13-Si12-O14	107.03	106.96	106.98
O11-Si11-O13	103.65	101.76	102.77	O13-Si12-O15	110.22	112.78	114.00
O11-Si11-O22	110.74	112.58	113.36	O13-Si12-O24	107.32	105.55	104.58
O12-Si11-O13	111.67	113.91	114.65	O14-Si12-O15	110.40	108.67	106.28
O12-Si11-O22	109.83	109.74	109.46	O14-Si12-O24	111.03	114.60	116.35
O13-Si11-O22	110.59	109.97	110.71	O15-Si12-O24	110.47	108.02	108.71
average	109.41	109.39	109.41	average	109.41	109.43	109.47
O-Si22-O (°)				O-Si23-O (°)			
O14-Si22-O23	109.24	108.81	108.89	O16-Si23-O21	110.66	109.11	107.48
O14-Si22-O24	111.48	107.07	107.58	O16-Si23-O25	106.56	105.64	104.63
O14-Si22-O25	108.08	114.83	115.00	O16-Si23-O26	111.12	114.43	119.79
O23-Si22-O24	109.75	114.12	115.08	O21-Si23-O25	113.34	114.24	117.28
O23-Si22-O25	110.79	106.69	105.58	O21-Si23-O26	107.87	106.87	104.96
O24-Si22-O25	107.24	105.07	104.51	O25-Si23-O26	106.99	106.45	103.05
average	109.42	109.43	109.44	average	109.42	109.46	109.53
O-Al13-O (°)				O-Al21-O (°)			
O11-Al13-O15	116.90	118.21	126.49	O12-Al21-O21	108.28	111.05	109.98
O11-Al13-O16	106.37	107.54	108.79	O12-Al21-O22	108.73	106.74	107.49
O11-Al13-O26	107.64	106.04	99.88	O12-Al21-O23	113.17	114.18	116.63
O15-Al13-O16	109.01	106.33	100.74	O21-Al21-O22	107.72	107.53	105.57
O15-Al13-O26	107.54	106.03	105.17	O21-Al21-O23	105.01	103.62	107.54
O16-Al13-O26	108.83	112.28	116.18	O22-Al21-O23	113.22	113.05	108.52
average	109.38	109.41	109.52	average	109.36	109.36	109.36
T-O-T (°)				T-O-T (°)			
Si11-O11-Al13	127.62	125.31	118.68	Si23-O21-Al21	130.96	127.20	125.05
Si11-O12-Al21	125.22	119.45	120.71	Si11-O22-Al21	125.62	121.81	121.24
Si11-O13-Si12	141.11	129.59	128.21	Si22-O23-Al21	139.30	128.77	130.37
Si12-O14-Si22	138.25	131.71	129.71	Si12-O24-Si22	135.68	128.11	124.86
Si12-O15-Al13	138.16	125.45	121.87	Si22-O25-Si23	139.05	127.32	123.93
Si23-O16-Al13	130.78	123.66	118.11	Si23-O26-Al13	132.45	126.61	120.51

TABLE 5. Geometry of LiO_4 tetrahedra

	1 atm	5.7 GPa	9.0GPa
Li1-O (Å)			
Li1-O11	2.026	1.961	1.911
Li1-O12	2.027	1.968	1.936
Li1-O16	2.024	1.992	1.961
Li1-O17	2.054	1.996	1.896
average	2.033	1.979	1.926
Li2-O (Å)			
Li2-O21	2.006	1.953	1.918
Li2-O22	2.008	1.971	1.941
Li2-O26	1.987	1.978	1.971
Li2-O27	2.021	1.978	1.939
average	2.005	1.970	1.942
O-Li1-O(°)			
O11-Li1-O12	101.5	98.5	96.7
O11-Li1-O16	103.4	102.3	103.5
O11-Li1-O17	121.6	128.5	121.8
O12-Li1-O16	105.1	107.6	106.0
O12-Li1-O17	109.9	112.8	120.9
O16-Li1-O17	112.2	103.8	104.5
average	109.0	108.9	108.9
O-Li2-O(°)			
O21-Li2-O22	103.4	98.3	94.5
O21-Li2-O26	106.8	106.1	112.4
O21-Li2-O27	120.1	123.3	110.6
O22-Li2-O26	109.3	110.4	110.5
O22-Li2-O27	108.0	112.5	117.9
O26-Li2-O27	107.5	104.2	108.5
average	109.2	109.1	109.1

TABLE 6. Geometry of water molecules and chain

	1 atm	5.7 GPa	9.0 GPa
O-H (Å)			
H11-O17	0.992	0.996	0.990
H12-O17	0.998	1.005	1.004
H21-O27	0.982	0.986	0.985
H22-O27	1.000	1.011	1.007
average	0.993	0.999	0.996
H-O-H (°)			
H12-O17-H11	102.7	103.5	104.8
H22-O27-H21	104.7	105.7	107.4
average	103.5	104.6	106.1
O(water)···H (Å)			
H12-O27	1.900	1.693	1.737
H22-017	1.872	1.735	1.701
average	1.886	1.714	1.719
O(frame)···H (Å)			
H11-O26	3.625	2.932	2.163
H11-O15	2.265	1.885	2.079
H21-O25	2.564	2.081	2.144
H21-O23	2.823	2.756	2.513
O···O (Å)			
O17-O27	2.831	2.680	2.657
O···H-O (°)			
O17-H22-O27	166.0	159.7	155.6
O27-H12-O17	174.6	163.8	160.1
average	170.3	161.7	157.9
O···O···O (°)			
O17-O27-O17	122.9	126.6	126.6

plane. It is noteworthy that the same behavior is also shown (as previously discussed) by the pyroxene chain, which runs parallel to the water chain.

The behavior of the intermolecular O····H distances is more involved, with apparent anomalies (see Table 6). Indeed, the contraction along *b* is also accompanied by significant, but not monotonic, shortening of the inter water O_{water}····H bonds.

These features can be explained by pointing out that the main aspect of the *P*-induced modifications on the water bonding system in bikitaite is the early formation of hydrogen bonds

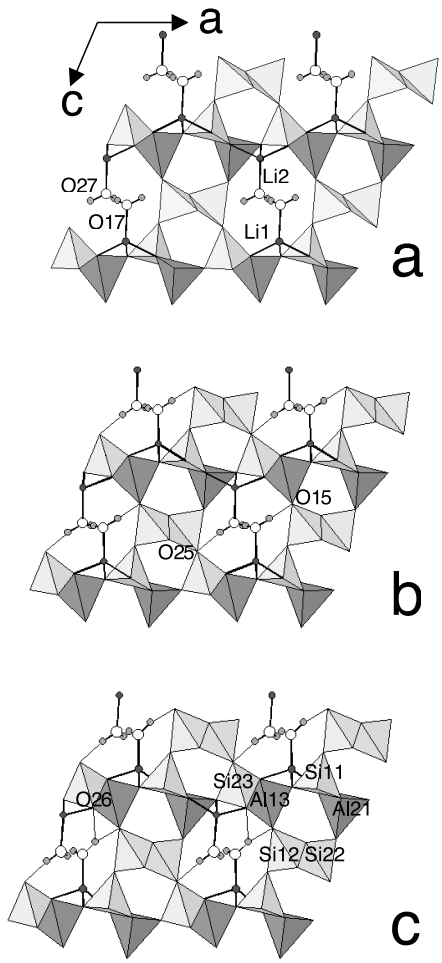

FIGURE 3. Projection along [010] of the bikitaite structure at P_{amb} (MD), 5.7 and 9 GPa.

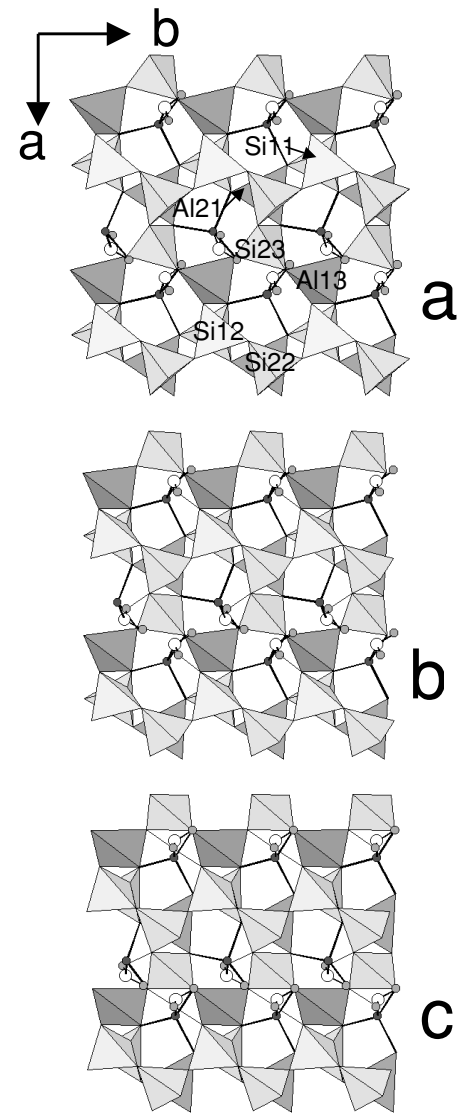

FIGURE 4. Projection along [001] of the bikitaite structure at P_{amb} (MD), 5.7 and 9 GPa.

with framework O atoms, which takes place in the pressure range P_{amb}–5.7 GPa (Table 6). As a consequence, the presence in the channels of a "floating" one-dimensional water chain disappears at high pressure. In fact, compression along *a* and *c* moves the framework O atoms close enough to the water hydrogen atoms to allow formation of new hydrogen bonds, without destroying the one-dimensional chain. In order to analyze in detail this significant change, we calculated the radial distribution functions (rdf), which represent the probability of finding a pair of atoms at a given distance. For O_{water}····H and O_{frame}····H, these functions, reported in Figure 6, show that, although no peak is present in the O_{frame}···H rdf at ambient pressure (in agreement with the absence of water-framework hydrogen bonds), a peak appears around 1.8 Å at 5.7 GPa (2.0 Å at 9 GPa), showing that water molecules are now also hydrogen bonded with framework O atoms. At 9 GPa the peak corresponding to the water-framework O_{frame}····H is different in shape and position with respect to the one at 5.7 GPa, indicating a further structural difference: more framework O atoms are now close to the same proton, and different hydrogen bonds are possible.

This feature is proved by analysis of the MD trajectory at 9.0 GPa, in which it was observed that water molecules may partially rotate around their axes in such a way as to exchange the linking framework O atom. In other words, during the time evolution of the system, many hydrogen bonds break and form with O_{frame}. For example, H11, which at ambient pressure is too far from the framework to form hydrogen bonds, by 5.7 GPa forms a moderately strong hydrogen bond with the framework O atom O15 (see Table 6), whereas at 9.0 GPa at least two framework O atoms (O15 and O26) come within the range of distances typical of hydrogen bonds. A competition takes place between O15 and O26 for hydrogen bonding with H11 and, as a result, two weaker hydrogen bonds, on average, are formed by H11.

A further interesting feature of the structure at 9 GPa appears by analyzing the distances of H21 from the water O atom O27, and from the two closest framework O atoms O23 and

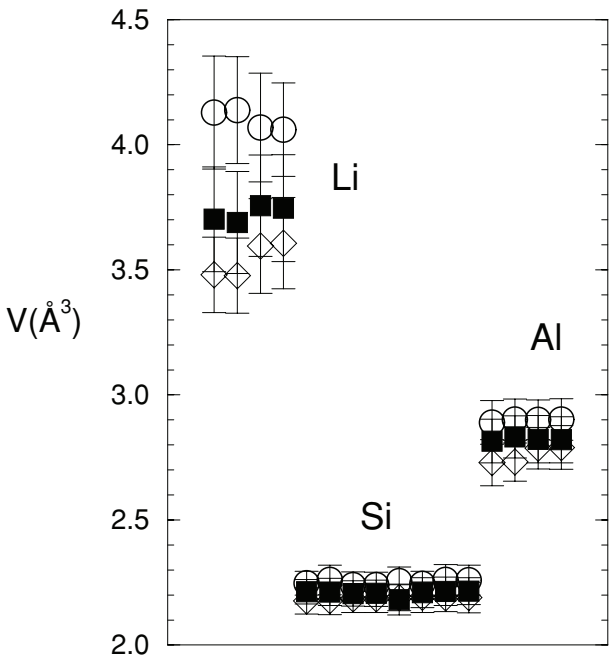

FIGURE 5. Tetrahedral volumes and error bars calculated at P_{amb}, 5.7 and 9 GPa. White circles represent the tetrahedral volumes at ambient pressure, black squares represent volumes at 5.7 GPa, white diamonds represent volumes at 9 GPa.

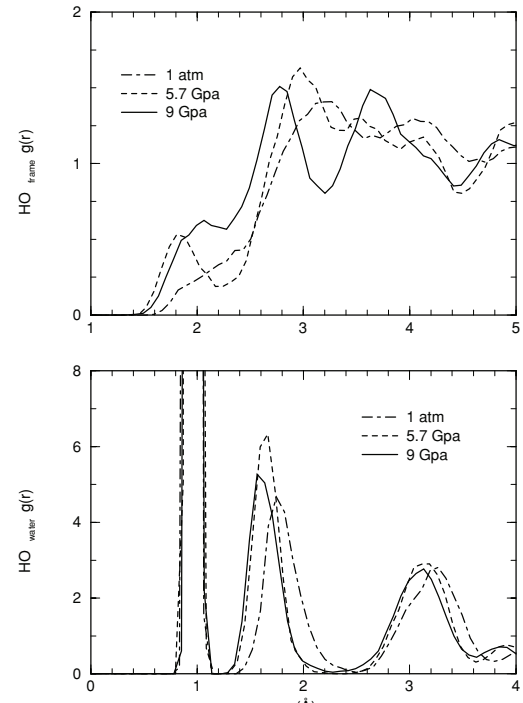

FIGURE 6. Radial distribution functions O_{water}····H e O_{frame}····H at the different pressures.

O25. These distances are reported in Figure 7. At about 1.0 ps, the distance from O23 falls abruptly to 1.36 Å, and the corresponding O23-O27 distance becomes 2.33 Å. As shown by the increase in oscillation of the H21-O27 bond distance, such an event significantly perturbs the water molecule. It can be argued that a further increase of pressure could bring the framework O atoms even closer to the water hydrogen atoms, and such a perturbation may well allow the breaking of the O-H bond, thus favoring a proton transfer to the bikitaite framework and the ionization of a guest water molecule. *P*-dependent vibrational spectroscopic studies, at frequencies characteristic of the intra- and intermolecular degrees of freedom of water, are planned for the future.

To our knowledge, experimental data on the dynamical behavior of water in bikitaite under H*P* are not available in literature. According to an ambient pressure 1H NMR study on bikitaite by Larsson et al. (1989), the dynamical process which mainly contributes to proton relaxation in the temperature range 224–418 K is a 180° rotation of the water molecule about its axis. The activation energy for such process, 30 KJ/mol (Larsson et al. 1989), is about one order of magnitude bigger than K*T* at 300 K, indicating that, at least for our MD simulation time scale, such a rotation is extremely improbable. As a consequence, we did not observe any 180° water rotations in the ambient pressure or H*P* simulations. However, a similar event was observed in an MD simulation of bikitaite at 363 K (work in preparation), where a water molecule rotates and exchanges the proton engaged in the water-water hydrogen bond.

DISCUSSION

The coordinates obtained by our calculations at 5.7 and 9.0 GPa were used to calculate theoretical powder patterns. They revealed a good correspondence with the experimental patterns and with those calculated using the GSAS program, confirming that no phase transition occurs in bikitaite during compression.

The experimentally determined modifications of the unit-cell parameters under H*P* can be interpreted from a structural point of view with the results of the MD simulations. Figure 2 shows that the *c* parameter undergoes the largest *P*-induced variation. This behavior can be interpreted by observing the projection of the bikitaite structure shown in Figure 3, which displays more circular 8-membered rings at high pressure: the two Li-O_{water} bond distances, which show the greatest reduction, are mainly oriented along *c*, thus affecting the structure in this direction. A further effect consistent with the decrease of the *c* parameter may be the formation of the hydrogen bond H11-O26, which, again, is approximately oriented along the *c* direction.

The *a* and *b* parameters show similar contractions with pressure. The main cause of contraction of *b* is the kinking of the pyroxene chain, which becomes more corrugated in the *bc* plane, as previously discussed. Along *a,* the structure can be described as a set of alternating layers characterized by different density: the less dense layers, containing the channels, are strongly deformed by the new interactions between the framework O atoms and the extraframework species. The other type of layer is less sensitive to the pressure change (Fig. 4). In or-

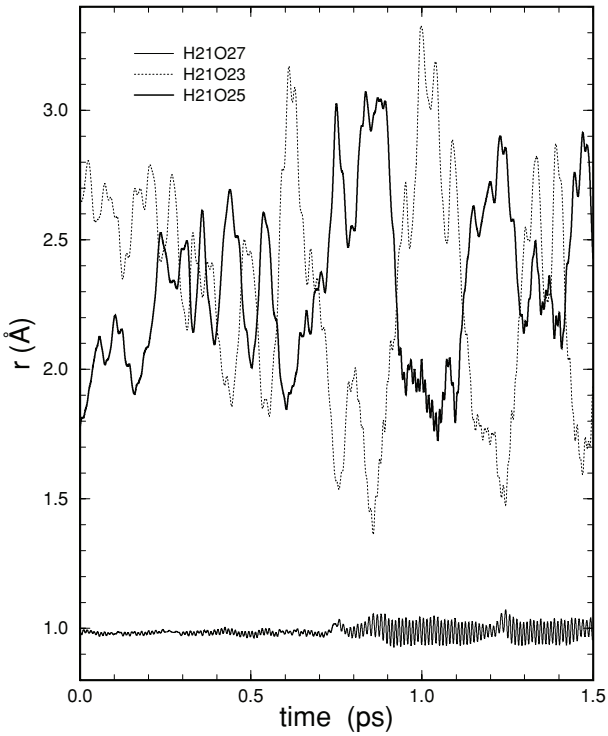

FIGURE 7. H11-O distances vs. time at 9 GPa.

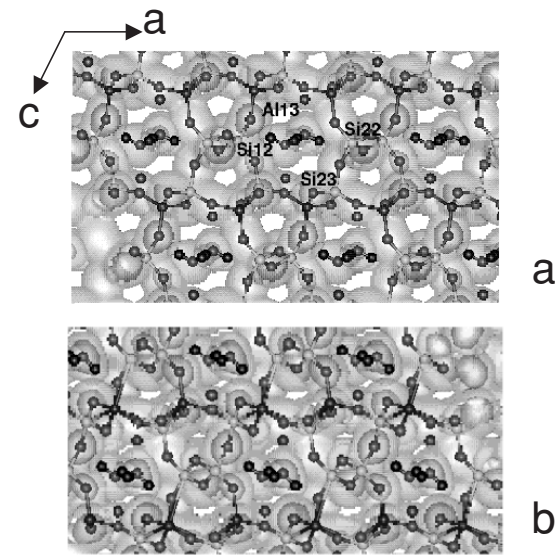

FIGURE 8. Contour plots of the electronic density of bikitaite at ambient pressure (**a**) and at 9.0 GPa (**b**) superimposed on the corresponding average bikitaite structure projected on the *ac* plane. Black spheres represent H atoms, light gray spheres Si atoms, gray spheres O atoms, and dark gray spheres Al and Li atoms. The gray shading indicates regions in which the electronic density is significantly different from 0; the darker the color, the higher the density.

der to understand the mechanism that is responsible at the atomic level for this type of distortion, we drew contour plots of the (valence) electronic density, projected on the *ac* plane, at room pressure and at 9.0 GPa (Fig. 8). As expected (because bikitaite is an insulator) electronic density is mainly localized along the T-O backbone and the O-H bonds of the water molecules. At room pressure, the electronic density minima are found in the zeolite channels. It is worth noticing that in the 8-membered rings, the electronic density is mainly localized along the *a* axis; in particular, regions of high density are found in the hexagonal sheets and in the layers containing water molecules and pyroxene chains. Figure 8 shows that the volume contraction occurring along the *c* axis, where the channel shows larger regions of low electron density, is favored with respect to an equivalent contraction along the *a* axis. Indeed, the latter deformation would bring about a larger superposition of electronic clouds; such an event is energetically unfavored due to electrostatic repulsion and, at shorter distances, would be forbidden by the exclusion principle. Moreover, the density distribution in the 8-ring channel is asymmetric, because much larger regions of low electron density are found along the longer channel's diagonal, although the electron density is more uniform along the shorter diagonal. On this basis it would be reasonable to say that in response to external pressure the lower density regions become full. In fact, if we examine the density contours at 9.0 GPa, rotation of the Si23 and Al13 tetrahedra results in partial filling of the low electronic density zones present in the 8-ring channels at ambient conditions. The rotation of the Si22 and Si12 tetrahedra, forming the pyroxene chains, results in filling of other low density regions (in the 5-membered rings; Fig. 8b).

With such rotations all the main holes are now occupied by atoms and further rotation of the other tetrahedra (i.e., Si11 and Al21) does not occur, probably because it would lead to an energetically unfavorable superposition of electronic densities. Therefore, we can conclude that, with applied pressure, the crystal structure deforms in such a way to avoid superposition of negatively charged regions. In the case of bikitaite, such a "minimum energy" deformation is achieved by rotations of quasi-rigid tetrahedra Si23, Al13, Si12, and Si22, involving T-O-T bond angles, which are more flexible than O-T-O angles and T-O bonds.

The other main response of bikitaite to pressure involves other relatively weak interactions: the Li-O coordination and the hydrogen bond structure.

In a recent work (Fois et al. 2001a) we demonstrated that the stability of the entropically unfavored one-dimensional arrangement of the water molecules in bikitaite at ambient pressure is due to the long range electrostatic interactions between the bikitaite acentric framework, characterized by a permanent dipole moment, and the water chains, which have a non zero *y* dipole component of opposite sign with respect to the framework. As no hydrogen bonds with framework O atoms are present, we concluded that the framework + water chain arrangement is stabilized by dipolar host-guest long range interactions. Because, as above discussed, volume contraction due to applied pressure causes the formation of additional hydro-

gen bonds with framework O atoms, it would be interesting to examine how the presence of these additional weak short-range interactions influences the stability of the zeolite. To this aim, we calculated the total energy of bikitaite as a whole, of the bikitaite framework without water molecules, and of the isolated water chain for the three pressure values. Then we examined how the stabilization energy of bikitaite (i.e., the difference between total energy and the sum of the energies calculated for the two separate sub-systems) changes with increasing pressure. Such results, as well as the dipole moments and polarization calculated for the three average bikitaite structures, are reported in Table 7. First, we notice that the total energy of bikitaite continuously increases with increasing pressures, in agreement with the fact that the structure at ambient pressure is the most stable and that, in order to distort such an arrangement, an external stress must be applied. Remarkably, the stabilization energy ΔE decreases with pressure, indicating that the maximum interaction energy between the water chain, the bikitaite framework, and the Li cations is obtained at ambient pressure. As shown in Table 7, the lowest interaction energy is in bikitaite at 9.0 GPa, notwithstanding the shorter Li-O water distance and the formation of additional hydrogen bonds. This can be justified by the decreasing contribution from the long-range dipolar interaction energy under application of an external pressure. In fact, as reported in Table 7, the total dipole moment of bikitaite decreases with pressure, and this decrease is mainly due to the framework dipole, which changes from 55.97 D at ambient pressure to 51.67 D at 9 GPa. This seems reasonable if we remember that the framework undergoes large distortions owing to rotations of Si23, Al13, Si12, and Si22 tetrahedra, thus affecting the value of the framework dipole moment.

It is interesting to compare the H*P*-behavior of bikitaite with that of other zeolites with different topology. The bulk modulus of bikitaite [K_0 = 45(1) GPa] is similar to those obtained, using non penetrating media, for analcime [K_0 = 41 GPa, Hazen and Finger 1979], scolecite [powder study, K_0 = 61(2) GPa, Ballone et al. 2002; single crystal study, K_0 = 54.6(3) GPa, Gatta et al. 2001], and natrolite [K_0 = 47(6) GPa, Goryainov and Smirnov 2001], and larger than those of heulandite [K_0 = 27.5(2) GPa, Comodi et al. 2001], and zeolite 4A [K_0 = 21 GPa, Hazen and Finger 1984]. The behavior of bikitaite with respect to amorphization is anomalous when compared with the other zeolites. In fact, notwithstanding the progressive *P*-induced long-range disorder, evidenced by the broadening of the powder pattern peaks of Figure 1, the zeolite is still crystalline up to about 10 GPa. These results confirm the high structural stability of bikitaite in non-ambient conditions. In addition, recent studies (Vezzalini et al. 2001b) still in progress, show that it is also stable up to very high temperature (about 900 °C), notwithstanding the complete dehydration occurring at about 450 °C. Moreover, the *T*-induced deformation of the bikitaite structure, even with completely empty channels, is much lower than that described here under high pressure. This behavior deviates from that observed for the other zeolites studied in detail up to now from a structural point of view under high *T* and high *P* (Alberti and Vezzalini 1983; Ståhl and Hanson 1994; Vezzalini et al. 2001a; Ballone et al. 2002). In general, the deformations are larger during dehydration, due to water loss and the consequently increased squeezability of the channels. Further studies are in progress on the H*P* behavior of anhydrous bikitaite, using penetrating and non-penetrating pressure-transmitting media.

ACKNOWLEDGMENTS

D. Levy is acknowledged for technical assistance during the in situ synchrotron XRPD experiments at beamline ID09, ESRF. The European Synchrotron Radiation Facility is kindly acknowledged for allocation of beam-time under proposal no CH-831. The authors thank M. Dove and an anonymous referee for the useful and constructive comments to the manuscript. This work was supported by Italian MIUR (COFIN2001 "Le zeoliti, materiali di interesse per l'industria e l'ambiente: sintesi, struttura, stabilità e applicazioni.") and CNR.

REFERENCES CITED

Alberti, A. and Vezzalini, G. (1983) The thermal behaviour of heulandites: structural study of the dehydration of Nadap heulandite. Tschermak Mineralogische Petrographische Mitteilungen, 31, 259–270.

Annehed, H. and Fälth, L. (1984) The crystal structure of $Cs_{0.35}Al_{0.35}Si_{2.65}O_6$, a cesium-aluminosilicate with the bikitaite framework. Zeitschrift für Kristallographie, 166, 301–306.

Ballone, P., Quartieri, S., Sani, A., and Vezzalini, G. (2002) High-pressure deformation mechanism in the zeolite scolecite: a combined computational-experimental study. American Mineralogy, 87, 1994–2006.

Baur, W.H. (1995) Framework mechanics: limits to the collapse of tetrahedral framework. In M. Rozwadowski, Ed., Proceedings 2nd Polish-German Zeolite Colloquium, p. 171–185. Nicholas Copernicus University Press, Torun, Poland.

Bazhan, I.S., Kholdeev, O.V., and Fursenko, B.A. (1999) Phase transformations in scolecite at high hydrostatic pressure. Doklady Akademy Nauk, 364, 97–100 (in Russian).

Becke, A.D. (1988) Density functional exchange energy approximation with correct asymptotic behaviour. Physical Review, A38, 3098–3100.

Belitsky, I.A., Fursenko, B.A., Gabuda, S.P., Kholdeev, O.V., and Seryotkin Yu.V. (1992) Structural transformations in natrolite and edingtonite. Physics and Chem-

TABLE 7. Calculated dipole moments, polarization and energies

	|μ|(D)	μ_x (D)	$_y(\mu_y)$(D)	$_z(\mu_z)$ (D)	P(C/m^2)	**E (au)**
1 atm						
bikitaite	47.35	–27.84	36.49	11.66	0.267	–497.502
$Li_4[Al_4Si_8O_{24}]$	55.97	–27.95	47.16	11.29		–428.426
$(H_2O)_4$	9.46	0.25	–9.46	0.06		–69.015
ΔE						–0.062
5.7 GPa						
bikitaite	44.06	–28.56	31.57	11.35	0.275	–497.444
$Li_4[Al_4Si_8O_{24}]$	53.46	–28.25	44.03	11.01		–428.375
$(H_2O)_4$	10.70	0.06	–10.70	0.00		–69.019
ΔE						–0.049
9.0 GPa						
bikitaite	44.41	–28.65	31.80	11.86	0.295	–497.357
$Li_4[Al_4Si_8O_{24}]$	51.67	–29.27	41.09	11.17		–428.312
$(H_2O)_4$	9.10	0.34	–9.09	0.18		–69.012
ΔE						–0.033

istry of Minerals, 18, 497–505.
Birch, F. (1952) Elasticity and constitution of the earth's interior. Journal of Geophysical Research, 57, 227–286.
Bish, D.L. (1995) Thermal behaviour of natural zeolites. In D.W. Ming and F.A. Mumpton, Eds., Natural Zeolites '93, 259–269. Brockpost, New York.
Bissert, G. and Liebau, F.N. (1986) The crystal structure of a triclinic bikitaite, $Li[AlSi_2O_6]\cdot H_2O$, with ordered Al/Si distribution. Neues Jahrbuch für Mineralogie Monatshefte, 6, 241–252.
Car, R. and Parrinello, M. (1985) Unified approach for molecular dynamics and density-functional theory. Physical Review Letters, 55, 2471–2474.
Comodi, P., Gatta, G. D., and Zanazzi, P.F. (2001) High-pressure structural behaviour of heulandite. European Journal of Mineralogy, 13, 497–505
Dove, M.T., Heine, V., and Hammonds, K.D. (1995) Rigid Unit Modes in framework silicates. Mineralogical Magazine, 59, 629–639.
Finger, L.W., Cox, D.E., and Jephcoat, A.P. (1994) A correction for powder diffraction peak asymmetry due to axial divergence, Journal of Applied Crystallography, 27, 892–900.
Fois, E., Tabacchi, G., Quartieri, S., and Vezzalini, G. (1999) Dipolar host/guest interactions and geometrical confinement at the basis of the stability of one-dimensional ice in zeolite bikitaite. Journal of Chemical Physics, 111, 355–359.
Fois, E., Gamba, A., Tabacchi, G., Quartieri, S., and Vezzalini, G. (2001a) Water molecules in single file: first-principles studies of one-dimensional water chains in zeolites. Journal of Physical Chemistry B, 105, 3012–3016.
———(2001b) On the collective properties of water molecules in one-dimensional zeolitic channels. Physical Chemistry Chemical Physics, 3, 4158–4163.
Gatta, G.D., Comodi, P., and Zanazzi, P.F. (2001) High-pressure structural behaviour of fibrous zeolites: the case of scolecite. Proceedings of GEOITALIA, 3° Forum FIST, 807–809, Abstract.
Gillet, P., Malézieux, J.M., and Itiè, J.P. (1996) Phase changes and amorphization of zeolites at high pressures: the case of scolecite and mesolite. American Mineralogist, 81, 651–657.
Goryainov, S.V. and Smirnov, M.B. (2001) Raman spectra and lattice-dynamical calculations of natrolite. European Journal of Mineralogy, 13, 507–519.
Goryainov, S.V., Fursenko, B.A., and Belitsky, I.A. (1996) Phase transitions in analcime and wairakite at low-high temperatures and high pressure. Physics and Chemistry of Minerals, 23, 297–298.
———(1999) Raman spectroscopy of phase transition and amorphyzation of wairakite at high pressure. Doklady Akademy Nauk, 369, 70–73.
Hammersley, A.P., Svensson, S.O., Hanfland, M., Fitch, A.N., and Häusermann, D. (1996) Two-dimensional detector software: from real detector to idealised image or two-theta scan. High Pressure Research, 14, 235–248.
Hammond, K.D., Heine, V., and Dove, M.T. (1997a) Insights into zeolite behaviour from the Rigid Unit Mode model. Phase Transitions, 61, 155–172.
Hammond, K.D., Deng, H., Heine, V., and Dove, M.T. (1997b) How floppy modes give rise to adsorption sites in zeolites. Physical Review Letters, 78, 3701–3704.
Hammond, K.D., Heine, V., and Dove, M.T. (1998) Rigid-Unit Modes and the quantitative determination of the flexibility possessed by zeolite frameworks. Journal of Physical Chemistry B, 102, 1759–1767.
Hazen, R.M. (1983) Zeolite molecular sieve 4A: anomalous compressibility and volume discontinuity at high pressure. Science, 219, 1065–1067.
Hazen, R.M. and Finger, L.W. (1979) Polyhedral tilting: a common type of pure displacive phase transition and its relationship to analcite at high pressure. Phase Transitions, 1, 1–22.
——— (1984) Compressibility of zeolite 4A is dependent on the molecular size of the hydrostatic pressure medium. Journal of Applied Physics, 56, 1838–1840.
Huang, Y. (1998) IR spectroscopic study of the effect of high pressure on zeolites Y, A and sodalite. Journal of Material Chemistry, 8, 1067–1071.
Hutter, J., Ballone, P., Bernasconi, M., Focher, P., Fois, E., Goedecker, S., Parrinello, M., and Tuckerman, M., (1990-1996) CPMD code 3.0; MPI (Stuttgart) and IBM Research (Zurich).
Kleinmann, L. and Bylander, D.M. (1982) Efficaceus form for model pseudopotentials. Physical Review Letters, 48, 1425–1428.
Kohn, W. (1999) Nobel Lecture: Electronic structure of matter. Wave functions and density functionals. Review of Modern Physics, 71, 1253–1266.
Kohn, W and Sham, L.J. (1965) Self-consistent equations including exchange and correlation effects. Physical Review A140, 1135–1141.
Larson, A.C. and Von Dreele, R.B. (1994) GSAS-General Structure Analysis System. Report LAUR 86-748, Los Alamos National Laboratory, Los Alamos, New Mexico.
Larsson, K., Tegenfeldt, J., and Kvick, Å. (1989) NMR study of the motion of water molecules in the natural zeolite bikitaite. Journal of Physics and Chemistry of Solids, 50, 107–110.
Le Bihan, T., Heathman, S., Darracq, S., Abraham, C., Winand, J-M., and Benedict, U. (1996) High pressure X-ray diffraction studies of UX3 (X = Al, Si, Ga, Ge, In, Sn). High Temperatures-High Pressures, 27/28, 157–162.
Lee, Y., Hriljac, J.A., Vogt, T., Parise, J.B., and Artioli, G. (2002) First structural investigation of a super hydrated zeolite. Journal of Physical Chemistry, 126, 5466–5475.
Mao, H.K., Xu, J., and Bell, P.M. (1986) Calibration of the ruby pressure gauge to 800 Kbar under quasi-hydrostatic conditions. Journal of Geophysical Research, 91, 4673–4676.
Moroz, N.K., Kholopov, E.V., Belitsky, I.A., and Fursenko, B.A. (2001) Pressure-enhanced molecular self-diffusion in microporous solids. Microporous and Mesoporous Materials, 42, 113–119.
Parrinello, M. (1997) From silicon to RNA: The coming of age of ab initio molecular dynamics. Solid State Communications, 102, 107–120.
Parrinello, M. and Rahman, A. (1981) Polymorphic transitions in single crystals: a new molecular dynamics method. Journal of Applied Physics, 52, 7182–7190.
Perdew, J.P. (1986) Density-functional approximation to the correlation energy of the inhomogeneus electron gas. Physical Review B, 33, 8822–8824.
Quartieri, S., Sani, A., Vezzalini, G., Galli, E., Fois, E., Gamba, A., and Tabacchi, G. (1999) One-dimensional ice in bikitaite: single-crystal X-ray diffraction, infrared spectroscopy and ab initio molecular dynamics studies. Microporous and Mesoporous Materials, 30, 77–87.
Ross, N.L. (2000) Franework structures. In R.M. Hazen and R.T. Downs, Eds., High-Temperature and High-Pressure Crystal Chemistry, vol. 41, p. 257–287. Reviews in Mineralogy and Geochemistry, Mineralogical Society of America, Washington, D.C.
Secco, R.A. and Huang, Y. (1999) Pressure-induced disorder in hydrated Na-A zeolite. Journal of Physics and Chemistry of Solids, 60, 999–1002.
Ståhl, K. and Hanson, J. (1994) Real-time synchrotron powder diffraction studies of the dehydration processes in scolecite and mesolite. Journal of Applied Crystallography, 27, 543–550.
Ståhl, K., Kvick, Å., and Ghose, S. (1989) One-dimensional water chain in the zeolite bikitaite: neutron diffraction study at 13 and 295K. Zeolites, 9, 303–311.
Thomson, P., Cox, D.E., and Hastings, J.B. (1987) Rietveld refinement of Debye-Scherrer synchrotron X-ray data from Al_2O_3. Journal of Applied Crystallography, 20, 79–83.
Troullier, N. and Martins, J.L. (1991) Efficient pseudopotentials for plane-wave calculations. Physical Review B, 43, 1993–2006.
Velde, B. and Besson, J.M. (1981) Raman spectra of analcime under pressure, Physics and Chemistry of Minerals, 7, 96–99.
Vezzalini, G., Quartieri, S., Sani, A., and Levy, D. (2001a) The structural modifications induced by high pressure in scolecite and heulandite: in-situ synchrotron X-ray powder diffraction study. In A. Galarneau, F. Di Renzo, F. Fajula, and J. Vedrine, Eds., Studies in surface sciences and catalysis, 135. Elsevier, Amsterdam.
Vezzalini, G., Ferro, O., Quartieri, S., Gualtieri, A.F., Cruciani, G., Fois, E., Ceriani, C., and Gamba, A. (2001b) Thermal behaviour and dehydration mechanism of bikitaite. Proceedings of the XIII International Zeolite Conference, Montpellier (France), July 8–13, 2001, abstract 09-R-04.

MANUSCRIPT RECEIVED FEBRUARY 12, 2002
MANUSCRIPT ACCEPTED MAY 11, 2002
MANUSCRIPT HANDLED BY ALISON R. PAWLEY